Nano-polycrystalline Ag-doped ZnO layer for steep-slope threshold switching selectors

Cite as: AIP Advances **11**, 115213 (2021); https://doi.org/10.1063/5.0066311
Submitted: 24 August 2021 • Accepted: 19 October 2021 • Published Online: 05 November 2021

Akshay Sahota, Harrison Sejoon Kim, Jaidah Mohan, et al.

Nano-polycrystalline Ag-doped ZnO layer for steep-slope threshold switching selectors

Cite as: AIP Advances 11, 115213 (2021); doi: 10.1063/5.0066311
Submitted: 24 August 2021 • Accepted: 19 October 2021 •
Published Online: 5 November 2021

View Online Export Citation CrossMark

Akshay Sahota,[1] Harrison Sejoon Kim,[2] Jaidah Mohan,[2] Dan N. Le,[2] Yong Chan Jung,[2] Si Joon Kim,[3,4] Jang-Sik Lee,[5] Jinho Ahn,[6,a)] Heber Hernandez-Arriaga,[2] and Jiyoung Kim[1,2,a)]

AFFILIATIONS

[1] Department of Electrical Engineering, The University of Texas at Dallas, 800 West Campbell Road, Richardson, Texas 75080, USA
[2] Department of Materials Science and Engineering, The University of Texas at Dallas, 800 West Campbell Road, Richardson, Texas 75080, USA
[3] Department of Electrical and Electronics Engineering, Kangwon National University, 1 Gangwondaehakgil, Chuncheon, Gangwon-do 24341, Republic of Korea
[4] Interdisciplinary Graduate Program in BIT Medical Convergence, Kangwon National University, 1 Gangwondaehakgil, Chuncheon-si, Gangwon-do 24341, Republic of Korea
[5] Department of Material Science and Engineering, Pohang University of Science and Technology (POSTECH), 77 Cheongam-ro, Pohang 790-784, Republic of Korea
[6] Division of Materials Science and Engineering, Hanyang University, 222 Wangshimni-ro, Seongdong-gu, Seoul 04763, Republic of Korea

[a)] **Authors to whom correspondence should be addressed:** jiyoung.kim@utdallas.edu and jhahn@hanyang.ac.kr

ABSTRACT

In this work, a nano-polycrystalline Ag-doped ZnO-based threshold switching (TS) selector via a facile co-sputtering technique is investigated without using an Ag active metal layer. The effects of the Ag concentration with respect to OFF-state leakage current (I_{off}) were studied, and the results demonstrate that by regulating the Ag doping concentration in the switching layer (SL), an electroforming-free switching with an I_{on}/I_{off} ratio of $\sim 10^8$ could be achieved, having an extremely low I_{off} value of $\sim 10^{-13}$ A. Furthermore, cycling endurance can also be improved as the formation of a laterally thick and stable filament does not happen promptly with consequent measurements when there is a limited amount of Ag in the SL. The selector device performance enhancement is attributed to the doping-based polycrystalline structure that facilitates enhanced control on filament formation due to the restricted availability and anisotropic diffusion of Ag ions in the polycrystalline ZnO SL, thereby trimming down the overall stochasticity during metallic filament growth. The present study demonstrates that a doping-based polycrystalline SL structure can be implemented in a selector device to augment TS characteristics, i.e., device variances and cycling endurance for adoption in ultra-high density memory applications.

I. INTRODUCTION

Recent breakthroughs in 3D cross (X)-point architecture arrays have put them in the spotlight for the studies related to implementing the next-generation high-density non-volatile memory technology for futuristic neuromorphic and stand-alone memory applications.[1–4] The 3D X-point structure fulfills the requirements of extremely high memory density using a simple device structure and also offers cost benefits in the memory industry owing to the 3D stacking viability, thereby lessening bit cost per memory chip.[5–8] However, an X-point architecture suffers from an inevitable issue of the sneak leakage path that is detrimental for its practical application as it increases overall power consumption and amplifies the read/write disturbance.[8–12] Thus, developing a selector device that prevents the sneak current for an unselected cell within an X-point array is required to mitigate this issue. An ideal selector device should inhibit any leakage current through the unselected cells offering high resistance at low bias, while turning on after crossing certain threshold voltage (V_{th}), enabling current flow for the selected memory cell.[13] A lot of selector devices

have been engineered until now to satisfy the X-point architectural requirements,[8,14,15] but among them, threshold switching (TS) selectors, namely, metal–insulator transition (MIT) selectors,[16,17] ovonic threshold switching (OTS) selectors,[18,19] and Ag (or Cu)-based steep-slope TS selectors,[20–24] have garnered much attention. MIT and OTS selectors, despite having exceptional endurance and reliability, suffer from a big flaw of high I_{off} (~10^{-7} A), which makes them unsuitable for next generation high-density memory applications.[8,9,25,26] Ag-based steep-slope TS selectors alternately outshine all other selector devices due to their exceptional features, such as extremely low leakage current (<1 pA), high I_{on}/I_{off} ratio (>10^7), small subthreshold swing (<10 mV/decade), and high current density (>1 MA/cm^2), yet they have a simple metal–insulator–metal (MIM) structure.[20,22,27–29]

The traditional approach of Ag-based TS selector fabrication involves depositing individual layers of metal oxide and Ag active reservoir electrode to form a MIM stack where the Ag electrode provides metal ions to the oxide layer for conductive filament formation once sufficient operational voltage (>V_{th}) is applied to the device. However, as this conduction mechanism of metallic filament formation in an active reservoir electrode-based system has a stochastic nature, it gives rise to unavoidable intrinsic variabilities.[30,31] Hence, parameter variability, e.g., shifts in V_{th}, and poor cycling endurance are inherent issues predominantly found in active reservoir electrode-based TS selectors.[32] The majority of the prevailing selector devices have an amorphous switching layer (SL) structure,[33–40] thus commanding isotropic diffusion of Ag ions, incorporating randomness. Another undesirable factor in Ag-based TS selectors is the necessity of the electroforming (EF) process that requires higher applied voltage than the operating voltage.[41] During the EF process, large Ag clusters having several nanometers of diameter are formed, which do not diffuse out completely from the conductive path when applied voltage is removed, and these residual Ag clusters thus lead to high I_{off} in the subsequent OFF-state, causing significant device performance deterioration.[21,27,41] TS selectors suffer from the issue of having non-volatile filament formations at high ON-currents possibly due to uncatered supply of Ag ions from the active reservoir electrode to the SL, leading to memory switching behavior, which is unpreferable for a selector device.[42–45] Metal doping[22,41,46,47] is thus one of the methods that has been adopted to inhibit the active metal ion over-injection, but the understanding of the operational mechanism per dopant concentration still remains unclear.

In our previous studies, TS selectors fabricated via the electrochemical deposition (ECD) process have been discussed,[22,46,47] but a big drawback of the ECD process is difficulties in film thickness precision and smooth film growth, thereby leading to non-reproducible results.[48–51] In addition, the solution-based ECD process is not desirable for executing conventional fabrication processes in the semiconductor industry. The sputtering method, on contrary, is an extensively used thin film deposition method employed by coating industries due to its capability to deposit large-scale metal-oxide films, simultaneously offering excellent controllability of thickness and doping concentration by simply adjusting the sputter target power and deposition conditions.[52–56] Hence, in this work, we present a metal-filament type TS selector with a novel doping-based nano-polycrystalline structure using the RF magnetron co-sputtering process. ZnO has been specifically chosen as the SL in our study because of its workability when doped with Ag;[46] hence, the crystalline ZnO SL with the preferred *c*-axis (002) orientation can be conveniently deposited via the RF magnetron co-sputtering technique.[57–59] Doping helps to regulate the influx of Ag ions during filament growth, while ZnO in its crystalline phase (wurtzite) allows facile anisotropic diffusion of Ag ions.[60,61] Although the literature studies using a multilayer selector structure to limit active metal ion influx mentioning reliability and endurance improvements are available,[52,62] a selector employing a polycrystalline SL has rarely been reported. The presented doping-based nano-polycrystalline TS selector shows the enhanced TS characteristics of extremely low I_{off} (~10^{-13} A), high I_{on}/I_{off} ratio (~10^8), and improved cycling endurance and does not require the EF process. The results demonstrate that the doping-based polycrystalline structure holds the potential to be utilized in selector devices for ultra-high density memory applications, such as 3D X-point arrays.

II. EXPERIMENTAL

We fabricated Ag-doped nano-polycrystalline ZnO-based (Pt/Ag-doped ZnO/Pt) TS selector devices by using 250 nm via-hole structures on a Si wafer. The detailed procedure for 250 nm via-hole structure fabrication has already been discussed elsewhere.[46] A Pt layer was used as the bottom contact electrode. Ag-doped ZnO served as the SL of the steep-slope TS selector devices and was deposited using the ATC Orion (by AJA International) sputter deposition system. The Ag doping-based amorphous ZnO SL was deposited using the ZnO target (Kurt J. Lesker, 99.9% purity) at a RF power of ~150 W and the Ag target (Kurt J. Lesker, 99.9% purity) at a DC power of ~27 W at room temperature. The Ag doping-based polycrystalline ZnO layer was deposited under the same conditions except for the ZnO target sputtered at ~250 W. For the evaluation of Ag concentration effects, the Ag doping-based polycrystalline ZnO layer was deposited at room temperature by co-sputtering the ZnO target at a RF power of ~250 W and the Ag:ZnO (ZnO/Ag 90/10 at. %; SCI Engineered Materials, 99.99% purity) composite target at varied RF powers (~50 W–~150 W). The Ag concentration has been tuned by adjusting the Ag:ZnO composite target power. The deposition thickness for the SL was ~30 nm. A 30 nm thick Pt layer was deposited via an e-beam evaporator (Temescal 1800) using a shadow mask, which served as the top contact electrode. The surface of fabricated thin films was characterized using x-ray diffraction (XRD, Rigaku SmartLab), x-ray photoelectron spectroscopy (XPS, PHI Versa Probe II), and scanning electron microscopy (SEM, Zeiss Supra 40). The Keithley 4200A-SCS parameter analyzer was used to evaluate electrical properties.

III. RESULTS AND DISCUSSION

Figure 1(a) shows the schematic process flow for Ag-doped nano-polycrystalline ZnO-based TS selector device fabrication. Figures 1(b) and 1(c) show the cross-sectional SEM image of the TS selector device without the Pt top electrode (TE) and the top view of selector devices with the TE, respectively. Figures 2(a) and 2(b) show the comparative analysis of the volatile switching characteristics between the selector devices having an amorphous and a polycrystalline ZnO SL, respectively. For the case of the Ag-doped amorphous ZnO SL, no TS behavior was observed with the non-ideal

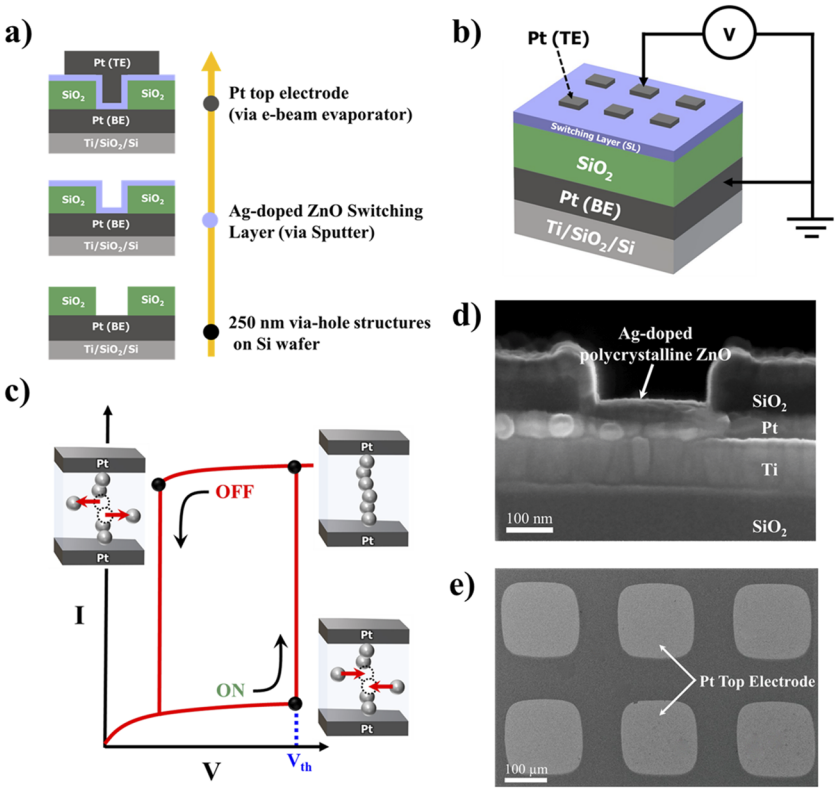

FIG. 1. (a) Schematic illustration of the selector device fabrication process flow, (b) electrical measurement scheme for a selector device, (c) example *I–V* curve of a threshold switching selector showing filament formation and rupturing with respective voltage sweeps, (d) cross-sectional SEM image of the Ag-doped nano-polycrystalline ZnO-based threshold switching selector device, and (e) top view of the threshold switching selector devices with the Pt top electrode.

device performance of selectors exhibiting the stuck-OFF state, i.e., continuous high resistance state. It is possibly due to Ag acting as an interstitial dopant in the amorphous SL instead of occupying substitutional sites,[63] which results in random walk or isotropic diffusion of Ag ions, thus making it difficult to form a conductive filament in the amorphous SL on the application of voltage bias. On contrary, Ag-doped polycrystalline ZnO-based selector devices showed EF-free TS characteristics with a tight threshold voltage (V_{th}) distribution having V_{th} standard deviation (SD) of ±0.05 V. These results are in good agreement with our earlier proposed hypothesis that crystalline ZnO allows facile anisotropic diffusion of Ag ions,[60,61] thereby reducing the V_{th} variabilities.[52,62] However, the Ag-doped polycrystalline ZnO-based TS selector devices showed a high leakage current I_{off} value (~10^{-9} A), and the presence of strong (100) and (101) peaks [Fig. 2(b), inset] indicates suppressed crystallinity with no preferred orientation possibly due to the higher Ag concentration of ~12 at. %, thereby giving the scope for further improving switching characteristics by reducing the Ag doping concentration in the ZnO SL.

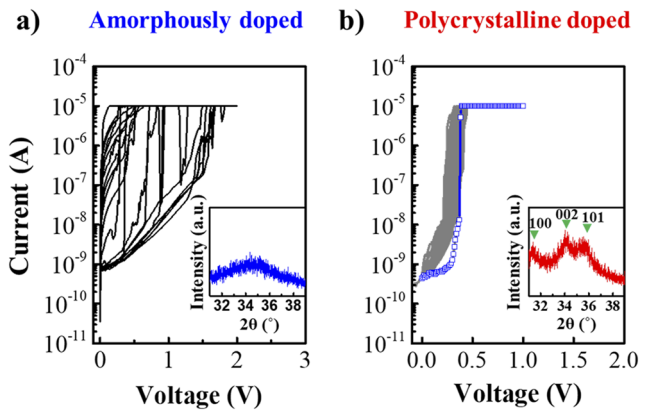

FIG. 2. Representative volatile switching characteristics of the selector devices deposited: (a) amorphously, displaying no threshold switching characteristics, and (b) polycrystalline, showing threshold switching characteristics (the blue line represents the first DC cycle); images in the inset show x-ray diffraction (XRD) patterns showing amorphously doped ZnO and polycrystalline doped ZnO, respectively. The Ag concentration in both cases is ~12 at. %.

Figures 3(a) and 3(b) demonstrate the physical and chemical properties of sputtered Ag-doped polycrystalline ZnO thin films deposited with very low Ag concentrations (~1–3 at. %). Figure 3(a) ratifies that all the sputtered ZnO thin films lightly doped with Ag have a polycrystalline phase with the preferred *c*-axis (002) orientation, which implies that doped ZnO maintains its wurtzite structure when slightly doped even without any thermal treatment. Thus, depositing the ZnO SL with low Ag concentration levels reasonably enhances the crystallinity of the SL. The lattice parameters for the Ag-doped ZnO case do not show any significant changes because of the most stable Ag substitution at the Zn site (Ag_{Zn}) dopant state as compared to AgO (Ag substitution at the O site) or Ag_i (Ag interstitial), which induces considerable lattice distortions as per the

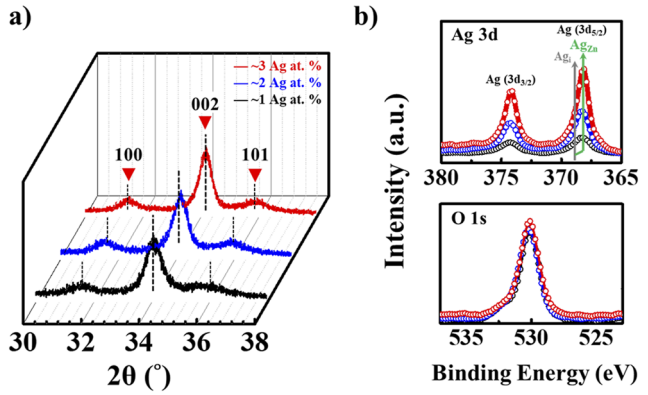

FIG. 3. (a) X-ray diffraction (XRD) patterns showing the preferred (002) orientation and (b) x-ray photoelectron spectroscopy (XPS) spectra of Ag $3d_{3/2}$ and Ag $3d_{5/2}$ (Ag_{Zn}) and O 1s of the Ag-doped ZnO films at varying Ag concentrations of ~1 at. % (black line), ~2 at. % (blue line), and ~3 at. % (red line).

calculations based on the density functional theory (DFT).[56] Figure 3(b) shows the XPS analysis performed to confirm the chemical state of doped Ag in the ZnO matrix. In Ag 3d spectra, the $3d_{5/2}$ peak is positioned at 368.2 eV for metallic Ag/Ag_i, whereas the binding energy for Ag^+ in Ag_{Zn} is positioned 0.5–0.7 eV lower.[56,64] The XPS analysis of Ag 3d and O 1s narrow scans shows the dominant Ag_{Zn} dopant state and thus demonstrates that the ZnO wurtzite structure has been successfully doped with substitutional Ag at Zn sites (the XPS spectra of Zn 2p and Ag 3d are shown in Fig. S1–S2).

Figure 4 shows the comparative analysis of volatile switching characteristics of non-Ag-based, Ag active reservoir electrode-based, and Ag-doping-based steep-slope TS selectors. Direct current (DC)–voltage (I–V) sweeps measured for five different types of TS devices show evident characteristics. No TS behavior was observed in the non-Ag-based ZnO device that is neither Ag-doped nor contains an Ag active reservoir electrode [Fig. 4(a)]. On the incorporation of an Ag active reservoir electrode, the selector device starts exhibiting TS behavior following the EF process in its pristine state [Fig. 4(b)]. The device current reaches the compliance current (I_{cc}) at the voltage of 2.72 ± 0.12 V during the EF process (the initial first voltage sweep), and thereafter, the selector device continuously showed TS behavior even at a switching voltage lower than the forming voltage. However, the TS selector device shows degraded properties in terms of high leakage current (I_{off}, ~10^{-8} A) and significant V_{th} variability (0.47 ± 0.33 V). It has been discussed earlier that I_{off} increases after the EF process due to the existence of Ag clusters,[41] and V_{th} variability is observed possibly because the growth of the metallic filament is a stochastic process (or a random event of multiple filament occurrence).[22,30] On the other hand, I_{off} for devices having an Ag-doped (~1 at. %) polycrystalline ZnO SL [Fig. 4(c)] was observed to dramatically subside by ~10^4 times as compared to that for the TS selectors containing an Ag active reservoir electrode. When the Ag concentration is varied in the polycrystalline ZnO SL from 1 to 3 at. %, the I_{off} value further decreases by a magnitude of 10 [Figs. 4(c)–4(e)]. The underlying phenomenon responsible for trimming down the I_{off} has been discussed in the next paragraph. Table I summarizes various switching parameters obtained for the TS selector devices discussed in Figs. 4(c)–4(e). It can be observed that although increasing the Ag concentration offers an indirect means to achieve V_{th} tunability and to lower I_{off}, an overall superior device performance is realized for the lowest Ag concentration of ~1 at. % considering DC cycling endurance and device yield potentially because of less lattice distortions induced in the ZnO wurtzite structure by the Ag dopant.

TABLE I. Summary of Ag-doped polycrystalline ZnO TS selector device parameters at varied Ag concentrations.

	Ag (~1 at. %)	Ag (~2 at. %)	Ag (~3 at. %)
Selectivity (I_{on}/I_{off})	~10^7	~10^7	~10^8
I_{off} (A)	~10^{-12}	~10^{-12}	~10^{-13}
V_{th} (V)	0.40	0.64	1.18
DC cycling endurance	>100 cycles	~10–15 cycles	<10 cycles
Device yield	~50%	~30%	~30%

Figures 5(a) and 5(b) show the statistical box chart for the device-to-device analysis of V_{th} and I_{off} distributions for the varied Ag concentration in Ag-doping-based steep-slope TS selectors.

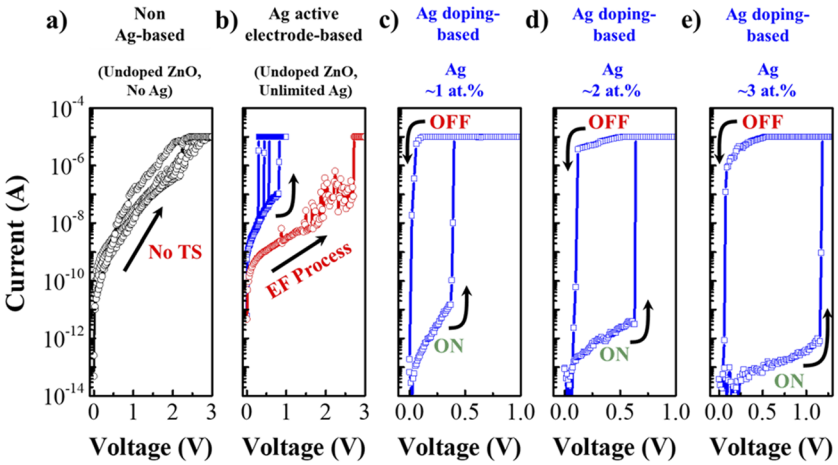

FIG. 4. Representative volatile switching characteristics of the fabricated devices: (a) non-Ag-based (highly insulating state) and (b) Ag active electrode-based, showing the EF process and subsequent TS behavior. The volatile switching characteristics depend on the Ag concentration: (c) ~1 at. %, (d) ~2 at. %, and (e) ~3 at. %, showing no EF process. The threshold voltages of (c)–(e) are 0.40, 0.64, and 1.18 V, respectively. Black arrows indicate the measurement direction. The SL is undoped for (a) and (b) and doped with Ag for (c)–(e).

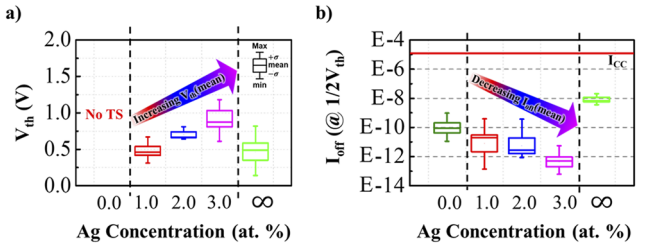

FIG. 5. Statistical analysis box chart of (a) threshold voltage and (b) leakage current, with varying Ag concentrations, showing mean values, standard deviations, and min/max outliers.

For each Ag concentration case, we tested at least ten devices and measured a minimum of 10 DC-*IV* cycles per device. Device-to-device V_{th} [Fig. 5(a)] for the infinite Ag amount case, i.e., Ag active reservoir electrode-based TS devices, displays a V_{th} SD of ±0.23 V, whereas for Ag doping-based ZnO TS devices by choosing a lightly doped selector medium (~1–3 at. %), V_{th} SD could be minimized to ±0.07 V. As mentioned earlier, the source of V_{th} variability in Ag active reservoir electrode-based TS devices is the stochastic nature of the metallic filament nucleation process,[30,31] whereas the reduction in V_{th} variability in the Ag-doping-based steep-slope TS selector case could be attributed to fewer low resistance paths available for filament growth,[22,65,66] constrained by doping. Interestingly, V_{th} (mean) was observed to increase when the Ag concentration was increased from 1 to 3 at. % for which the thermal energy involved during filament formation might be responsible, although a thorough investigation on V_{th} shifting with the increasing Ag concentration is imperative for more clarity. Figure 5(b) shows extremely high I_{off} (~10 nA) for all the measured Ag active reservoir electrode-based selector devices. However, for Ag-doping-based steep-slope TS devices, fewer than 40% of the measured devices show a leakage current of ~0.1 nA and 20% devices showed I_{off} with a magnitude of ~10 pA, while the remaining devices exhibited an I_{off} value of ~1 pA or lower. This is because of the shifting of the Fermi level toward the valance band edge owing to Ag_{Zn} that acts as a shallow acceptor in the ZnO wurtzite structure, eventually curtailing I_{off}.[22,56,67–69] Ultimately, TS selector devices with extremely low leakage current (~10 fA), high I_{on}/I_{off} ratio (~10^8), and extremely small subthreshold swing/switching slope (<1 mV/decade) can be realized.

Based on the DC cycling endurance studies on the Ag active reservoir electrode-based and Ag-doping-based steep-slope TS devices, a noteworthy difference in the number of DC cycles sustained before TS device fails is noticed. Ag active reservoir electrode-based TS devices show a continuous stuck-ON state (i.e., low resistance state) even for less than 10 DC cycles, while for the Ag doping-based TS devices, more than 100 consecutive DC cycles (Fig. S3) could be acquired before the device goes into a permanent stuck-ON state. For the Ag active reservoir electrode-based TS devices, the plausible explanation is because of the unrestrained supply of Ag ions from the Ag active reservoir electrode, the successive radial growth of the metallic filament is easier, which leads to laterally thick and stable filament formation, thereby leading to a permanent stuck-ON state. However, for the Ag doping-based TS devices, the radial growth of the metallic filament is subdued by slight doping of Ag in the polycrystalline ZnO selector medium.

IV. CONCLUSION

In this study, we fabricated a doping-based polycrystalline metal-filament type TS selector that facilitated enhanced control on filament formation due to the restricted availability and anisotropic diffusion of Ag ions in the polycrystalline ZnO SL. TS characteristics were found to be improved compared to those of the selector devices with the amorphous ZnO SL. The effects of the Ag concentration with respect to I_{off} were investigated for the Ag doping-based TS selectors having different Ag concentrations. An impressive 99.99% reduction in I_{off} is observed when Ag is introduced as a dopant in the polycrystalline ZnO matrix, which is attributed to Ag that serves as a *p*-type dopant, thus balancing the intrinsically *n*-type nature of ZnO, and lowers down I_{off}. In addition, doping the selector medium eliminates the requirement of the EF process, which otherwise leads to degraded device performance as evident from Ag active reservoir electrode-based TS selectors where the EF process is vital. I_{off} for Ag doping-based (~1 at. %) TS selectors was found to be reduced by an order of 4 as compared to that of the Ag active reservoir electrode-based TS selectors. By varying the Ag concentration from 1 to 3 at. %, I_{off} further tends to drop by one order and an I_{on}/I_{off} ratio of ~10^8 can be achieved. Moreover, device-to-device V_{th} distribution for Ag doping-based TS shows merely a SD of ±0.07 V. The reduced V_{th} variability is ascribed to only a few low resistance paths available for filament growth. It has been demonstrated that with the Ag doping approach, DC cycling endurance could be augmented as doping strictly confines the Ag concentration in the ZnO SL, thus impeding the successive growth of the metallic filament. Additionally, it was noticed that the doping-based polycrystalline SL could potentially help in providing a better control over V_{th} for TS devices. Finally, our study provides a simple and efficient way to realize excellent TS behavior by implementing a doping-based polycrystalline structure, which could pave the way for developing robust 3D X-point and neuromorphic circuits.

SUPPLEMENTARY MATERIAL

See the supplementary material for the XPS spectra of Zn 2p and Ag 3d peaks and representative volatile switching *I*–*V* characteristics of Ag ~1 at. % showing >100 DC cycling loops.

ACKNOWLEDGMENTS

This work was partially supported by the Semiconductor Research Corporation (SRC) through the GRC-LMD Program (Project No. 2823.001) and, in part, by the 2019 Research Grant from Kangwon National University. The authors would like to appreciate helpful discussions made with project liaisons I. V. Karpov (Intel), D. Ahn (Samsung Electronics), J. Han (SK hynix), J. Song (SK hynix), B. M. Kope (TSMC), X. Bao (TSMC), S. Vaziri (TSMC), and Y. S. Chen (TSMC).

AUTHOR DECLARATIONS

Conflict of Interest

The authors have no conflicts to disclose.

DATA AVAILABILITY

The data that support the findings of this study are available from the corresponding author upon reasonable request.

REFERENCES

[1] K. Roy, A. Jaiswal, and P. Panda, Nature **575**, 607 (2019).
[2] S. Yu, Proc. IEEE **106**, 260 (2018).
[3] Z. Wang, H. Wu, G. W. Burr, C. S. Hwang, K. L. Wang, Q. Xia, and J. J. Yang, Nat. Rev. Mater. **5**, 173 (2020).
[4] S. Salahuddin, K. Ni, and S. Datta, Nat. Electron. **1**, 442 (2018).
[5] K. Takeuchi, in *Proceedings of IEEE International Symposium on Circuits and Systems* (IEEE, 2014), Vol. 1046.
[6] K. Bakshi, in *Proceedings of the IEEE Aerospace Conference* (IEEE, 2012), Vol. 1.
[7] H. Zhang, G. Chen, B. C. Ooi, K.-L. Tan, and M. Zhang, IEEE Trans. Knowl. Data Eng. **27**, 1920 (2015).
[8] G. W. Burr, R. S. Shenoy, K. Virwani, P. Narayanan, A. Padilla, B. Kurdi, and H. Hwang, J. Vac. Sci. Technol. B **32**, 040802 (2014).
[9] J. Y. Seok, S. J. Song, J. H. Yoon, K. J. Yoon, T. H. Park, D. E. Kwon, H. Lim, G. H. Kim, D. S. Jeong, and C. S. Hwang, Adv. Funct. Mater. **24**, 5316 (2014).
[10] L. Zhang, S. Cosemans, D. J. Wouters, G. Groeseneken, M. Jurczak, and B. Govoreanu, IEEE Trans. Electron Devices **62**, 3250 (2015).
[11] S. H. Jo, T. Kumar, S. Narayanan, W. D. Lu, and H. Nazarian, in Techical Digest—International Electron Devices Meeting IEDM 6.7.1, 2015.
[12] S. H. Jo, T. Kumar, S. Narayanan, and H. Nazarian, IEEE Trans. Electron Devices **62**, 3477 (2015).
[13] Y. Koo and H. Hwang, Sci. Rep. **8**, 11822 (2018).
[14] R. Aluguri and T.-Y. Tseng, J. Electron Devices Soc. **4**, 294 (2016).
[15] A. Chen, J. Comput. Electron. **16**, 1186 (2017).
[16] M. Son, J. Lee, J. Park, J. Shin, G. Choi, S. Jung, W. Lee, S. Kim, S. Park, and H. Hwang, IEEE Electron Device Lett. **32**, 1579 (2011).
[17] S. Kim, X. Liu, J. Park, S. Jung, W. Lee, J. Woo, J. Shin, G. Choi, C. Cho, S. Park, D. Lee, E. J. Cha, B. H. Lee, H. D. Lee, S. G. Kim, S. Chung, and H. Hwang, in *Digest of Technical Papers—Symposium on VLSI Technology* (IEEE, 2012), Vol. 155.
[18] M. J. Lee, D. Lee, H. Kim, H. S. Choi, J. B. Park, H. G. Kim, Y. K. Cha, U. I. Chung, I. K. Yoo, and K. Kim, in *International Electron Devices Meeting IEDM Technical Digest* (IEEE, 2012), Vol. 2, p. 33.
[19] S. Kim, Y. B. Kim, K. M. Kim, S. J. Kim, S. R. Lee, M. Chang, E. Cho, M. J. Lee, D. Lee, C. J. Kim, U. I. Chung, and I. K. Yoo, in *Digest of Technical Papers—Symposium on VLSI Technology* (IEEE, 2013), Vol. 9.
[20] R. Midya, Z. Wang, J. Zhang, S. E. Savel'ev, C. Li, M. Rao, M. H. Jang, S. Joshi, H. Jiang, P. Lin, K. Norris, N. Ge, Q. Wu, M. Barnell, Z. Li, H. L. Xin, R. S. Williams, Q. Xia, and J. J. Yang, Adv. Mater. **29**, 1604457 (2017).
[21] Z. Wang, S. Joshi, S. E. Savel'ev, H. Jiang, R. Midya, P. Lin, M. Hu, N. Ge, J. P. Strachan, Z. Li, Q. Wu, M. Barnell, G.-L. Li, H. L. Xin, R. S. Williams, Q. Xia, and J. J. Yang, Nat. Mater. **16**, 101 (2017).
[22] H. S. Kim, A. Sahota, J. Mohan, A. T. Lucero, Y. Chan Jung, M. Kim, J.-S. Lee, R. Choi, S. J. Kim, and J. Kim, ACS Appl. Electron. Mater. **3**, 2309 (2021).
[23] J. Woo, D. Lee, E. Cha, S. Lee, S. Park, and H. Hwang, IEEE Electron Device Lett. **35**, 60 (2014).
[24] T. Liu, M. Verma, Y. Kang, and M. Orlowski, Appl. Phys. Lett. **101**, 073510 (2012).
[25] Z. Wang, S. Kumar, R. S. Williams, Y. Nishi, and H.-S. P. Wong, Appl. Phys. Lett. **114**, 183501 (2019).
[26] H.-Y. Li, X.-D. Huang, J.-H. Yuan, Y.-F. Lu, T.-Q. Wan, Y. Li, K.-H. Xue, Y.-H. He, M. Xu, H. Tong, and X.-S. Miao, Adv. Electron. Mater. **6**, 2000309 (2020).
[27] Z. Wang, M. Rao, R. Midya, S. Joshi, H. Jiang, P. Lin, W. Song, S. Asapu, Y. Zhuo, C. Li, H. Wu, Q. Xia, and J. J. Yang, Adv. Funct. Mater. **28**, 1870036 (2018).
[28] J. Song, J. Woo, A. Prakash, D. Lee, and H. Hwang, IEEE Electron Device Lett. **36**, 681 (2015).
[29] J. Park, J. Yoo, J. Song, C. Sung, and H. Hwang, IEEE Electron Device Lett. **39**, 1171 (2018).
[30] R. Waser, R. Dittmann, G. Staikov, and K. Szot, Adv. Mater. **21**, 2632 (2009).
[31] I. Valov, R. Waser, J. R. Jameson, and M. N. Kozicki, Nanotechnology **22**, 254003 (2011).
[32] W. Sun, B. Gao, M. Chi, Q. Xia, J. J. Yang, H. Qian, and H. Wu, Nat. Commun. **10**, 3453 (2019).
[33] S. Li, X. Liu, S. K. Nandi, and R. G. Elliman, Nanotechnology **29**, 375705 (2018).
[34] R. Sengottaiyan, N. Saxena, and K. D. Shukla, Semicond. Sci. Technol. **36**, 015013 (2020).
[35] A. Verdy, F. d'Acapito, J. B. Dory, G. Navarro, M. Bernard, and P. Noé, Phys. Status Solidi RRL **14**, 1900548 (2020).
[36] J. Y. Raty and P. Noé, Phys. Status Solidi RRL **14**, 1900581 (2020).
[37] J. Yoo, J. Woo, J. Song, and H. Hwang, AIP Adv. **5**, 127221 (2015).
[38] H. W. Ahn, D. S. Jeong, B. K. Cheong, S. D. Kim, S. Y. Shin, H. Lim, D. Kim, and S. Lee, ECS Solid State Lett. **2**, N31 (2013).
[39] D. Lee, T. Kim, and H. Sohn, Appl. Phys. Express **12**, 085504 (2019).
[40] J. A. J. Rupp, R. Waser, and D. J. Wouters, IEEE Xplore **7**, 1–4 (2016).
[41] W. H. Jeong, J. H. Han, and B. J. Choi, Nanoscale Res. Lett. **15**, 27 (2020).
[42] J. Song, J. Woo, J. Yoo, S. A. Chekol, S. Lim, C. Sung, and H. Hwang, IEEE Trans. Electron Devices **64**, 4763 (2017).
[43] Q. Hua, H. Wu, B. Gao, M. Zhao, Y. Li, X. Li, X. Hou, M. F. (Marvin) Chang, P. Zhou, and H. Qian, Adv. Sci. **6**, 1900024 (2019).
[44] J. Van Den Hurk, E. Linn, H. Zhang, R. Waser, and I. Valov, Nanotechnology **25**, 425202 (2014).
[45] T. Hino, T. Hasegawa, H. Tanaka, T. Tsuruoka, K. Terabe, T. Ogawa, and M. Aono, Nanotechnology **24**, 384006 (2013).
[46] U.-B. Han, D. Lee, and J.-S. Lee, NPG Asia Mater. **9**, e351 (2017).
[47] Y. Park, U. Bin Han, M. K. Kim, and J. S. Lee, Adv. Electron. Mater. **4**, 1700521 (2018).
[48] V. A. Myamlin and Y. V. Pleskov, *Electrochemistry of Semiconductors* (Noyes Publications, 1967).
[49] A. A. Ojo and I. M. Dharmadasa, Coatings **8**, 262 (2018).
[50] T. D. Golden, M. G. Shumsky, Y. Zhou, R. A. VanderWerf, R. A. Van Leeuwen, and J. A. Switzer, Chem. Mater. **8**, 2499 (1996).
[51] Y. Yamaguchi, M. Yamazaki, S. Yoshihara, and T. Shirakashi, J. Electroanal. Chem. **442**, 1 (1998).
[52] Y. Sun, X. Zhao, C. Song, K. Xu, Y. Xi, J. Yin, Z. Wang, X. Zhou, X. Chen, G. Shi, H. Lv, Q. Liu, F. Zeng, X. Zhong, H. Wu, M. Liu, and F. Pan, Adv. Funct. Mater. **29**, 1970081 (2019).
[53] J. H. Park, D. Kim, D. Y. Kang, D. S. Jeon, and T. G. Kim, ACS Appl. Mater. Interfaces **11**, 29408 (2019).
[54] R. Francq, R. Snyders, and P.-A. Cormier, Vacuum **137**, 1 (2017).
[55] J. Musil, P. Baroch, J. Vlček, K. H. Nam, and J. G. Han, Thin Solid Films **475**, 208 (2005).
[56] M. A. Thomas, W. W. Sun, and J. B. Cui, J. Phys. Chem. C **116**, 6383 (2012).
[57] R. C. Chang, S. V. Chu, K. Y. Lo, S. C. Lo, and Y. R. Huang, Integr. Ferroelectr. **69**, 43 (2005).
[58] A. K. Jazmati and B. Abdallah, Mater. Res. **21**, 1 (2018).
[59] S. Kunj and K. Sreenivas, AIP Conf. Proc. **1731**, 080048 (2016).
[60] G. Y. Huang, C. Y. Wang, and J. T. Wang, J. Phys.: Condens. Matter **21**, 195403 (2009).
[61] P. Erhart and K. Albe, Appl. Phys. Lett. **88**, 201918 (2006).
[62] K. J. Gan, W. C. Chang, P. T. Liu, and S. M. Sze, Appl. Phys. Lett. **115**, 143501 (2019).
[63] N. Shukla, B. Grisafe, R. K. Ghosh, N. Jao, A. Aziz, J. Frougier, M. Jerry, S. Sonde, S. Rouvimov, T. Orlova, S. Gupta, and S. Datta, in Techical Digest—International Electron Devices Meeting IEDM 34. 6.1, 2017.
[64] S. W. Gaarenstroom and N. Winograd, J. Chem. Phys. **67**, 3500 (1977).
[65] Q. Liu, S. Long, H. Lv, W. Wang, J. Niu, Z. Huo, J. Chen, and M. Liu, ACS Nano **4**, 6162 (2010).
[66] B. Song, R. Cao, H. Xu, S. Liu, H. Liu, and Q. Li, Nanomaterials **9**, 408 (2019).
[67] Y. Yan, M. M. Al-Jassim, and S. H. Wei, Appl. Phys. Lett. **89**, 181912 (2006).
[68] M. Shahrokhi and R. Moradian, Indian J. Phys. **89**, 249 (2015).
[69] O. Volnianska, P. Boguslawski, J. Kaczkowski, P. Jakubas, A. Jezierski, and E. Kaminska, Phys. Rev. B **80**, 245212 (2009).